Materials Advances

ROYAL SOCIETY OF CHEMISTRY

PAPER

View Article Online
View Journal | View Issue

Cite this: *Mater. Adv.*, 2025, 6, 3104

Sorafenib nanocrystals enhance bioavailability and overcome multidrug resistance in liver cancer cells: an approach based on *P*-gp inhibition strategy

Mohamed Nasr, *[ab] Sameh Saber,[c] Heba I. Elagamy,[b] Soha M. El-Masry,[d] Haydy Asad,[e] Ahmed A. E. Mourad,[f] Ahmed Gaafar Ahmed Gaafar[f] and Shaimaa K. Mostafa[b]

This research aimed to improve the oral bioavailability of Sorafenib (SF) and overcome multidrug resistance in hepatocellular carcinoma cells based on *P*-glycoprotein (*P*-gp) inhibition strategy. Four nanocrystal formulations (F1–F4) were developed using Labrasol® (LB) or Gelucire® (GL) as stabilizers as well as *P*-gp inhibitors. The prepared SF nanocrystal (SF-NC) formulations were characterized *in vitro* and *in vivo*. The results of *in vitro* studies showed that LB-based nanocrystals (F2) prepared using 0.02% LB, significantly reduced the crystal size and improved the aqueous saturation solubility of SF compared to the GL-based nanocrystals. Crystal morphology analysis of SF-NC (F2) revealed a uniform arrangement of nanosized crystals with significantly smaller particle size compared to plain SF. Furthermore, *in vitro* cytotoxicity studies showed that LB had no significant effects on cell viability of MDR-HepG2 and SF-resistant Huh-7 cells and can be considered safe in the *in vivo* environment at concentrations more than 10 times its corresponding concentration in SF-NC. However, LB-stabilized SF-NC significantly reduced IC_{50} values in MDR-HepG2 and SF-resistant Huh-7 cells compared to plain SF. *In vivo* absorption studies revealed that SF-NC significantly increased the rate and extent of absorption with a 1.27-fold increase in relative bioavailability. The developed SF-NC stabilized by LB as a *P*-gp inhibitor is expected to be a promising approach to improve oral bioavailability and restore SF's activity against multidrug-resistant hepatocellular carcinoma cells.

Received 10th February 2025,
Accepted 2nd April 2025

DOI: 10.1039/d5ma00122f

rsc.li/materials-advances

Introduction

Sorafenib tosylate (SF) is a multi-kinase inhibitor and is currently the only drug approved by the FDA for the treatment of advanced liver cancer.[1–3] It can facilitate apoptosis, attenuate angiogenesis, suppress tumor cell proliferation, and improve overall survival by approximately three months compared to a placebo. However, SF's clinical efficacy is hindered by the limited oral absorption from the gastrointestinal tract, which is primarily due to the poor aqueous solubility and its classification as a *P*-gp substrate.[4,5]

P-gp is only overexpressed in certain kinds of cancers and carries a lot of anticancer medications, which makes the malignancies resistant to those medications.[6] The decrease in antitumor drug intracellular concentration is due to drug efflux by *P*-glycoprotein (*P*-gp) which is considered a key factor contributing to the development of MDR in cancer cells.[7] Previous reports indicated that the therapeutic anticancer efficacy of SF relies on various efflux transporters, such as *P*-glycoprotein (*P*-gp),[8–11] multidrug resistance-associated proteins 2 and 3 (MRP2 and 3), breast cancer resistance protein (BCRP), organic anion transporting polypeptide 1B1/3 (OATP1B1/3), and organic cation transporter-1 (OCT1). These efflux transporters play a key role in cancer chemoresistance[8,12–15] due to the efflux extrusion of either SF itself or its metabolites, which show chemical characteristics typical of *P*-gp and MRP2 substrates.[16–18] Accordingly, a potential reduction of its intracellular concentration and therapeutic efficacy could be expected.[15] Previous reports indicated that *P*-gp was

[a] *Department of Pharmaceutics and Industrial Pharmacy, Faculty of Pharmacy, Helwan University, Cairo 11790, Egypt. E-mail: m2nasr@yahoo.com*
[b] *Department of Pharmaceutics, Faculty of Pharmacy, Delta University for Science and Technology, Gamasa 11152, Egypt*
[c] *Department of Pharmacology, Faculty of Pharmacy, Delta University for Science and Technology, Gamasa 11152, Egypt*
[d] *Department of Pharmaceutics, Faculty of Pharmacy, Damanhour University, Damanhour 22511, Egypt*
[e] *Drug analysis and chromatography research lab, Faculty of Pharmacy, Delta University for Science and Technology, Gamasa 11152, Egypt*
[f] *Department of Pharmacology and Toxicology, Faculty of Pharmacy, Port Said University, Port Said 42511, Egypt*

involved in the transport of SF, and coadministration with *P*-gp inhibitors like verapamil[10] or morphine[9] could increase SF absorption in either Caco-2 cell model or rats.

Several formulation approaches have been applied to overcome SF's poor water solubility to improve its bioavailability, such as cyclodextrin-based inclusion complex,[19] solid self-nano-emulsifying drug delivery systems,[20] liquid nanocrystals,[21] solid dispersion,[22] mesoporous solid dispersion,[23] in addition to nanoparticle-based drug delivery systems, including liposomes,[24,25] polymeric nanoparticles,[26–28] polyethylene glycol nanoparticles,[29,30] nanostructured lipid carriers,[31,32] silica nanoparticles,[33,34] and solid lipid nanoparticles.[1,35–37]

Nanocrystals or solid micelles are commonly employed as a formulation strategy to enhance the solubility of poorly water-soluble drugs by increasing the surface area available for dissolution and subsequently enhancing the bioavailability.[38] Drug nanocrystals consist of solid drug particles surrounded by a stabilizer layer, preventing individual particles' aggregation. Various stabilizers have been utilized in the stabilization of nanocrystals such as polymers like hydroxypropyl methylcellulose, polyvinylpyrrolidone K30, and Pluronic® as well as amphiphilic surfactants like polysorbates,[39] Labrasol,[40] and sodium lauryl sulfate.[41–43] Amphiphilic surfactants enhance the solubility of nanocrystals *via* better wetting and solubilizing effects. In addition to their solubilization effect, some stabilizers like LB, and Gelucire 44/14 (GL) have been found to possess inhibitory activity against efflux transporters, particularly *P*-gp.[44–46]

This study aimed to develop a novel SF-nanocrystals (SF-NC) by using LB or GL as stabilizers and *P*-gp inhibitors. The newly developed SF-NC will be *in vitro* and *in vivo* evaluated. *In vitro* characterizations of SF-NC include crystal characteristics, saturation aqueous solubility, dissolution, and cytotoxicity in terms of IC_{50} against resistant cancer cells compared to plain SF crystals. *In vivo*, the influence of SF-NC on oral absorption in rats will be evaluated. The developed SF-NC formulation is expected to be a promising approach to improve SF oral bioavailability and potentiate its activity against resistant cancer cells.

Materials and methods

Materials

Sorafenib tosylate was purchased from Cayman Chemical (Ann Arbor, MI, USA). Gelucire® 44/14 and Labrasol® (caprylocaproyl polyoxyl-8 glycerides) were kindly provided as a gift by Gattefosse, Saint-Priest Cedex, France. Acetonitrile (HPLC grade) was obtained from BDH, Poole, England. We bought methanol, phosphoric acid, sodium dihydrogen orthophosphate dihydrate (pharmaceutical quality), and hydrochloric acid (analytical grade) from El Nasr Chemical Company in Cairo, Egypt.

Methods

Preparation of SF-NC. Different SF-NC were prepared by recrystallization from acetone in the presence of different stabilizers. Four SF-NC formulations (F1–F4) were prepared using Labrasol® (LB) or Gelucire® 44/14 (GL) as stabilizers. Briefly, a solution of SF in acetone was prepared by heating to 60 °C. The prepared hot solution was injected in cold water containing different concentrations of the stabilizers. F1 and F2 were prepared using LB (0.01 and 0.02% w/v, respectively). GL was used in concentration of 0.01 and 0.02% w/v to stabilize F3 and F4 respectively. Plain SF crystals were prepared by the same procedure without using stabilizers. The prepared SF crystals were collected and dried at 50 °C.

Characterization of SF-NC

Particle size analysis. The prepared crystals were dispersed in a saturated solution of SF in deionized water at 25 ± 0.5 °C. The mean particle size and size distribution were determined using Zeta Sizer Nano-series (Nano ZS), Malvern, Worcestershire, UK. The measurements were conducted in triplicate, and the results were reported as the mean particle size ± standard deviation.

Saturation solubility. The determination of the saturated aqueous solubility of both plain SF crystals and SF-NC formulations involved the addition of surplus powder samples to 10 milliliters of deionized water in test tubes with airtight screws. The tubes were left on a water-bath shaker set to 25 °C for 48 hours in order to reach equilibrium. Five minutes at 3000 rpm were spent centrifuging the equilibrated samples. To quantify SF at 265 nm using spectrophotometry, aliquots of the supernatants were filtered through a 0.2 μm membrane filter and the filtrate was appropriately diluted with deionized water.[47] The mean and standard deviations of each sample were noted after it was evaluated in three copies.

Scanning electron microscopy (SEM). Electron micrographs of the chosen SF-NC and plain SF were taken with a scanning electron microscope (JEOL JSM-5500 LV-JEOL Ltd, Japan) operating in high vacuum. The samples were coated with a gold sputter coater (SPI-Module) prior to observation.

Differential scanning calorimetry (DSC). DSC was carried out on plain SF and SF-NC using a thermal analysis system (PerkinElmer Inc., Waltham, MA, USA) to detect any possible change in the physical state of SF-NC compared to plain ST. The samples (5 mg) were heated in an aluminum pan under a nitrogen environment at a constant rate of 10 °C min^{-1}. As a reference, a similar empty pan was used.

X-ray powder diffraction studies. Using an X-ray diffractometer (Shimadzu XRD 7000, Japan) with Cu as the tube anode, X-ray diffraction patterns of SF-NC and plain SF samples were obtained in order to verify the physical state of SF. The diffractograms were recorded at room temperature with the following parameters: 45 kV of voltage, 30 mA of current, 0.02° of (2°) steps, and 0.5 s per step counting rate. Data were collected between 4 and 40°2.

***In vitro* dissolution study.** The dissolution pattern of SF-NC and regular SF were contrasted. Using the Hanson dissolving apparatus (Hanson Research, California, USA), the dissolution studies were carried out in accordance with the paddle technique (USP). The temperature was kept at 37 °C ± 0.5 °C while the paddles rotated at 100 rpm. To maintain sink conditions, the

dissolution medium was 900 mL of 0.1 N HCl (pH = 1.2) with 0.1% tween.[48,49] 200 mg samples that had been precisely weighed were added to the dissolving medium. Samples of the dissolution medium (3 mL) were taken at various intervals, filtered through a 0.2 μm membrane filter, diluted accordingly, and then spectrophotometrically examined at 265 nm to determine the concentration of SF. New medium was used in place of the withdrawn samples. Three separate experiments were run for the dissolving processes.

Determination of LB content in SF-NC. LB content in SF-NC was determined by fluorimetry based on the fluorescence of caprylocaproyl polyoxyl-8 glycerides.[50] Samples of ST-NC (10 mg) were dissolved in 10 mL of ethanol. The obtained solutions were filtered through a 0.2 μm membrane. The filtrate was diluted with ethanol and analyzed for LB concentration using a Shimadzu spectro-fluorophotometer RF-6000 (Shimadzu, Kyoto, Japan). Using an excitation wavelength of 220 nm, the fluorescence intensity of LB solutions was evaluated at λ_{em} 295 nm against a reagent blank solution of ethanol that had undergone comparable treatment. All the assays were achieved at room temperature, applying a scan speed of 6000 nm min^{-1}, and keeping the bandwidth of the excitation and emission monochromators at 5 nm. A calibration curve of LB fluorescence intensity against concentrations (1–25 ng mL^{-1}) was utilized to estimate the amount of LB in SF-NC. Each sample was examined in triplicate.

***In vitro* cytotoxicity studies.** Multidrug-resistant HepG2 and SF-resistant Huh-7 cells were used to evaluate the *in vitro* cytotoxicity of SF-NC compared to plain SF. MDR-HepG2 cells were developed as previously described.[51] In summary, HepG2 cells were cultivated in RPMI-1640 media containing 10% (v/v) fetal bovine serum (FBS), 100 U mL^{-1} penicillin G, and 100 μg mL^{-1} streptomycin. The cells were then incubated at 37 °C in a humidified atmosphere of CO_2 and air. The cells were received from the American Type Culture Collection (ATCC). Following this, during cell passages, the cells were cultivated with varying amounts of Doxorubicin, ranging from 0.1 to 100 μM. Following multiple selection rounds, resistant HepG2 exhibiting MDR characteristics was discovered.[51] The developed resistant HepG2 cells by the same procedure were previously characterized by an overexpression of *P*-glycoprotein.[52,53]

The establishment of SF-resistant Huh-7 cell line was conducted according to the method described by Verslype, van Malenstein.[54] In summary, Huh-7 cells were cultured for 21 days straight in a medium containing 5 μM SF. Every three days, the medium containing SF was changed, and the cells were divided when they achieved 80% confluency. The developed SF-resistant Huh-7 cells were maintained in DMEM supplemented with 10% fetal bovine serum, 100 U mL^{-1} penicillin G, and 100 μg mL^{-1} streptomycin and kept in the 37 °C humidified CO_2 incubator. Previous reports indicated that resistance of hepatocellular carcinoma to SF was associated with increased expression of *P*-gp.[55,56]

Cell viability assay. MDR-HepG2 and SF-resistant Huh-7 cells were seeded in 96-well plates at the density of 1.5×10^4 cells per well and incubated for 24 hours. The cells were incubated for 24 h with 100 μL of different concentrations of either SF-plain, SF-plain + 50 μM verapamil as a standard *P*-gp inhibitor,[57] and SF-NC formulation (F2, stabilized by 0.1% LB). To evaluate the impact of LB exposure on the survival of MDR-HepG2 and SF-resistant Huh-7 cells, both kinds of cells were cultured in DMSO at different LB doses ranging from 1 to 10 ng mL^{-1} for a full day. To further clarify the treatment's cytotoxic effects, 0.1% DMSO was administered to the vehicle control groups. The MTT (3-(4,5-dimethylthiazol-2-yl)-2,5-diphenyltetrazolium bromide) assay was used to measure the vitality of the cells. In summary, 10 μL MTT per 100 μL media was incubated for an additional 3 hours at 37 °C in a humid environment with 5% CO_2. After dissolving the formazan in DMSO, the absorbance at 570 nm was measured.[58]

Bioavailability study

Study design. The Animal Ethics Committee of Delta University for Science and Technology's Faculty of Pharmacy has approved the protocol for animal studies (approval number: FPDU3/2024). Two groups of twelve mature male Wistar rats, weighing 200 g on average, were formed. All rats were given free access to water and were permitted to fast throughout the whole night. Each rat in groups 1 and 2 received a single dosage of 50 mg kg^{-1} of either plain SF or SF-NC aqueous suspension on the day of the experiment.

Plasma sample preparation. Blood samples were collected in heparinized tubes at different time intervals. The blood samples were centrifuged (Centrifuge, PLC-03, Gemmy Industrial Corporation, Taiwan) at 5000 rpm for 10 min; then transferred to Eppendorf tubes; and stored at −80 °C till analysis.

HPLC analysis of SF. The plasma concentrations of SF were determined using a validated HPLC-UV previously published method with minor modification.[59] The analysis was carried out on a reversed-phase column (Zorbax SB-C18) (2.1 mm × 100 mm i.d.; 1.8 Micron, Agilent, USA) at room. The mobile phase was 10 mM sodium dihydrogen orthophosphate dihydrate (pH = 3 adjusted using phosphoric acid) and acetonitrile in ratio of (55 : 45, v/v), pumped by a flow rate of 0.25 mL min^{-1}. The detection wavelength was 265 nm. The validity of the method was examined regarding selectivity, linearity, precision, and accuracy according to ICH guidelines.[60] SF plasma calibration curve was established by spiking 200 μL blank plasma with 20 μL of working standard solutions to obtain concentrations ranging from (1–1000 μg mL^{-1}) prepared by dilutions of stock of SF solution (1000 μg mL^{-1}) in HPLC methanol. Plasma samples (200 μL) were added to 20 μL Celecoxib solution (100 μg mL^{-1} in methanol, as an internal standard). To precipitate plasma proteins, 400 μL of acetonitrile was added. The resultant mixture was centrifuged (Tabletop Centrifuge, PLC-03, Gemmy Industrial Corporation, Taiwan) at 4000 rpm for 15 min and finally, the supernatant was filtered through 0.22 μm Millipore filter and 20 μL was injected into HPLC.

HPLC method was validated regarding selectivity, linearity, precision, and accuracy according to ICH guidelines. HPLC chromatogram of blank plasma, plasma spiked with SF, and celecoxib (internal standard) showed selectivity of the method

with no interferences with plasma components. From the SF calibration curve in plasma, the linearity was achieved over the concentration range of 1–1000 μg mL^{-1} with R^2 = 0.9976. Precision was 2.8702 to 9.458% and accuracy was 96.83 to 103.3% while inter-day precision was 0.178 to 8.034% and accuracy was 94.65 to 108.4%.

Bioavailability parameters. The rate and amount of medication absorption were evaluated between SF-NC and plain SF in terms of bioavailability characteristics. The concentration–time curve was used to determine the peak plasma concentration (C_{max}) and time (T_{max}). The linear trapezoidal rule was used to calculate the area under the curve (AUC0-24) to the latest quantified concentration of each group. The AUC_{0-24} of SF-NC was divided by the AUC_{0-24} of plain SF to determine the relative bioavailability.

Statistical analysis. For statistical analysis, GraphPad Prism 6 (California, USA) was utilized. The degree of statistical difference between the two data sets was assessed using the *t*-test. The data were shown as mean ± standard deviation (SD), and a statistically significant difference between the groups was defined as a *p*-value of less than 0.05.

Results and discussion

Characterization of SF-NC

Particle size. The size of particles plays a crucial role in determining the behavior of nanocrystals in drug delivery systems. The results of the prepared nanocrystal formulation and plain SF are presented in Table 1. The crystal size of plain SF was 893.80 ± 15.66 nm, however, when 0.01% and 0.02% w/v LB were used as a stabilizer, the particle sizes of nanocrystal formulations F1 and F2 were significantly reduced to 320.40 ± 8.86 and 132.30 ± 5.57 nm, respectively. On the other hand, when 0.01% and 0.02% w/v GL were used to stabilize the nanocrystals of F3 and F4 crystal sizes were 350.70 ± 9.69 nm and 310.90 ± 7.61 nm, respectively (Fig. 1). It is worth noting that all nanocrystal formulations exhibited a relatively low homogeneous size distribution, as indicated by the relatively high PDI values ranging from 0.445 to 0.937 (Table 1).

The results of particle size analysis indicated that a significant reduction in crystal size was achieved by using LB compared to the size of nanocrystals prepared by GL. This might be explained based on the surface activity of LB that can prevent agglomeration and promote the formation of smaller, more uniformly distributed nanocrystals.[61,62] On the other hand, GL, a combination of mono, di, triglycerides, and polyethylene glycol esters of fatty acids,

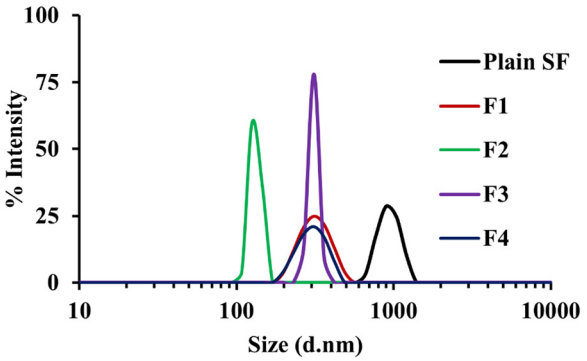

Fig. 1 Particle size distribution of plain SF and SF-NC formulations (F1 and F2 stabilized by 0.01% and 0.02% w/v LB, respectively, F3 and F4 were stabilized by 0.01% and 0.02% w/v GL, respectively).

stabilizes the formed crystals through the formation of gel phase or liquid crystals, which may limit particle size reduction.[63,64] Accordingly, it is believed that the higher solubilizing and surfactant properties of LB lead to a more prominent reduction in particle size than GL. The mechanism behind the particle size reduction by stabilizers like LB and GL implicates their surfactant characteristics. They are known to develop self-emulsifying systems, which are isotropic mixtures that form oil in water emulsions under mild stirring.[62] These systems can decrease the particle size of the drug effectively, thus improving its solubility and bioavailability.[63]

Solubility study. Table 1 shows the results of saturation aqueous solubility of plain SF and SF-NC formulations. The solubility of plain SF was 0.01 ± 0.003 μg mL^{-1}, this result is consistent with a previously reported study.[21] On the other hand, the aqueous solubility of SF-NC formulations was significantly increased to 2.00 ± 0.119, 4.45 ± 0.072, 1.69 ± 0.075, and 1.66 ± 0.081 μg mL^{-1} in case of F1, F2, F3, and F4 respectively. The notable increase in SF saturation solubility may be attributed to the higher surface area provided by reduced nanosized crystals. Moreover, the presence of traces of LB or GL on the surface of nanocrystal could enhance the wetting ability of nanocrystal formulations due to their surfactant characteristics compared to plain SF. Based on the results of saturation aqueous solubility and crystal size, F2 nanocrystal formulation was selected for further evaluation.

Crystal morphology. The morphology of plain SF and F2 nanocrystals was characterized by SEM. SEM image of plain SF (Fig. 2(A)) revealed irregular large particles. However, F2 nanocrystals (Fig. 2(B)) demonstrated uniform and organized arrangement of nanosized crystals.

Differential scanning calorimetry. The thermal behaviors of plain SF and SF-NC formulation (F2) were further characterized

Table 1 Stabilizers, particle size, polydispersity index (PDI), and saturated aqueous solubility of SF-NC formulations

	Stabilizer (concentration % w/v)	Particle size (nm ± SD, *n* = 3)	PDI	SF saturated aqueous solubility (μg mL^{-1} ± SD, *n* =3)
Plain SF	—	893.80 ± 15.66	0.937	0.01 ± 0.003
F1	LB (0.01)	320.40 ± 8.86	0.445	2.00 ± 0.119
F2	LB (0.02)	132.30 ± 5.57	0.641	4.45 ± 0.072
F3	GL (0.01)	350.70 ± 9.69	0.668	1.69 ± 0.075
F4	GL (0.02)	310.90 ± 7.61	0.603	1.66 ± 0.081

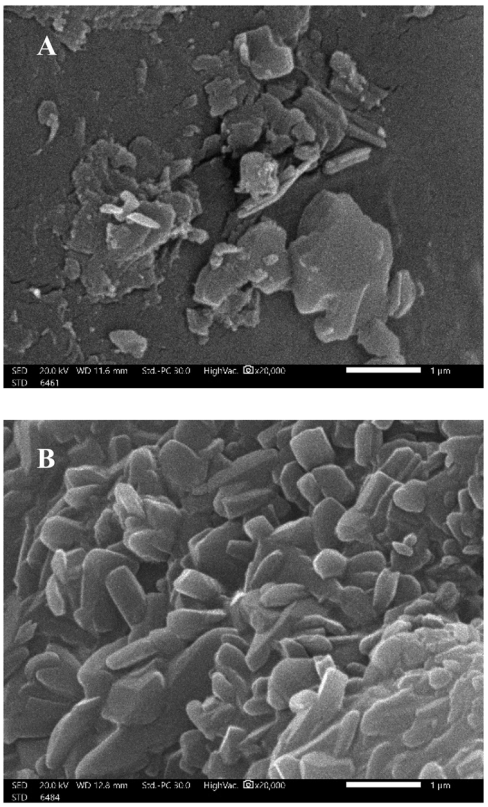

Fig. 2 SEM photographs of (A) plain SF and (B) F2 nanocrystals.

by DSC (Fig. 3). The thermogram of SF exhibited one large, sharp endothermic peak at about 217.99 °C representing the melting point of its tosylate salt form, in addition to a small endothermic peak at about 188 °C which might be relevant to the melting point of the SF base form. These findings were consistent with previous studies.[22] However, the thermogram of ST-NC showed a new sharp endothermic peak at 116 °C indicating the formation of a new crystalline structure. The newly formed polymorph of SF might be due to the interaction between amino groups of SF and the fatty acid esters in LB. The new polymorph of SF has a lower melting point than the drug itself that would boost drug solubility due to the reduction of the crystal lattice energy.

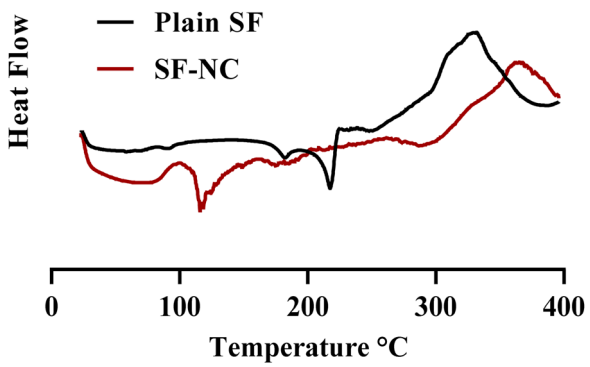

Fig. 3 DSC thermogram of plain SF and SF-NC formulations (F2).

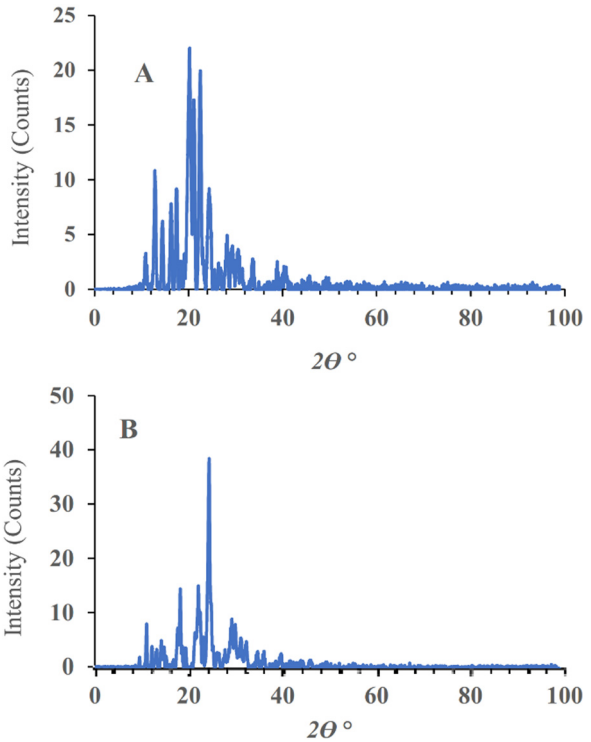

Fig. 4 Powder XRD patterns of plain-SF (A), and SF-NC (B).

Powder XRD. The crystallinity of the plain SF and SF-NC were determined by PXPD analysis. Typical diffraction patterns of plain SF and SF-NC are shown in Fig. 4. The diffraction pattern of SF showed various characteristic 2θ peaks at 12.6°, 14.2°, 15.7°,16.9°, 20.1°, 20.4°, 22.1°, 23.8°, 27.5°, 30.2° and 33.9°. However, these characteristic peaks were absent in the pattern of the SF-NC, and new peaks were observed at 10.6°, 11.5°, 12.3°, 13.4°, 13.9°, 14.4°, 17.2°, 18°, 18.5°, 21.8°, 22.3°, 24.2°, 25.2°, 28.4°, 30.3°, 31.3°, 33.8° and 35.1° indicating formation of new more crystalline structure. This finding is consistent with DSC findings.

***In vitro* dissolution study.** The dissolution profiles of SF and a representative nanocrystal formulation (F2) are shown in Fig. 5. F2 was selected based on its small particle size and the higher aqueous solubility compared to other nanocrystal formulations.

The values of dissolution parameters of plain SF including the % drug dissolved after 10 and 120 min ($Q_{10\%}$ and $Q_{120\%}$) were 25.22 ± 1.23 and 49.55 ± 1.44% compared to 90.12 ± 2.6 and 99.60 ± 1.55 in the case of F2 formulation, with dissolution efficiency % at 15 min (% DE_{15min}) of 25.23 ± 1.65 and 61.9 ± 2.31 for plain SF and F2 respectively. It was obvious that dissolution parameters were significantly higher for F2 compared to plain SF. This enhancement resulted from the solubilization effects of LB which improved SF wettability and hydrophilicity in dissolution media due to its amphiphilic characters and the reduced particle size. This leads to increasing drug surface area available for dissolution medium and subsequently, the dissolution velocity increases, as verified by the Noyes–Whitney equation.[65]

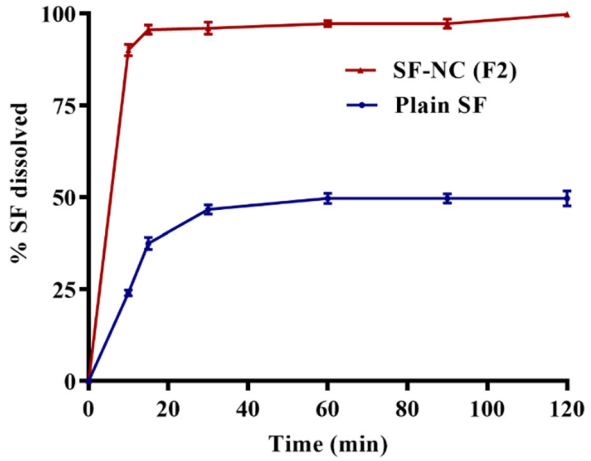

Fig. 5 *In vitro* dissolution profiles of SF-NC (F2) and plain SF.

***In vitro* cytotoxicity study.** To investigate the cytotoxic effects of LB on MDR HepG2 and SF-resistant Huh7 cells, both cell lines were subjected to various concentrations of LB ranging from 1 to 10 ng mL^{-1}. In this study, the concentration of LB was approximately 10-fold more than its concentration incorporated in SF-NC. LB content in SF-NC was determined by fluorimetry and was found to be 96.16 ± 12.34 ng mg^{-1}. In the cytotoxicity studies, the highest concentrations of SF and LB in the SF-NC were equivalent to 4.648 μg mL^{-1} and 0.446 ng mL^{-1}, respectively. The results in Fig. 6 indicate that, within the tested concentration range, LB did not cause significant cytotoxic effects in either MDR HepG2 or SF-resistant Huh7 cells. Previous work showed that including LB as an excipient in formulation of ravuconazole self-nano emulsifying system, at concentrations up to 5 nM had no significant effects on HepG2 cell viability and can be considered safe in the *in vivo* environment.[66]

Fig. 7(A) and (B) illustrates the results of cell viability of MDR HepG2 and SF-resistant Huh-7 cells after exposure to either SF-plain crystals or SF-NC formulation (F2), as well as SF-plain in addition to 50 μM verapamil. Table 2 summarizes the calculated IC_{50} values for each treatment. The IC_{50} values for SF-plain crystals were 9.60 ± 1.07 μM for MDR HepG2 cells and 10.67 ± 1.30 μM for SF-resistant Huh7 cells. In contrast, the IC_{50} values were significantly reduced to 6.31 ± 0.71 μM and 7.06 ± 0.84 μM, respectively, when using SF-NC, which may be attributed to the presence of LB as a *P*-gp inhibitor on the surface of SF-NC.

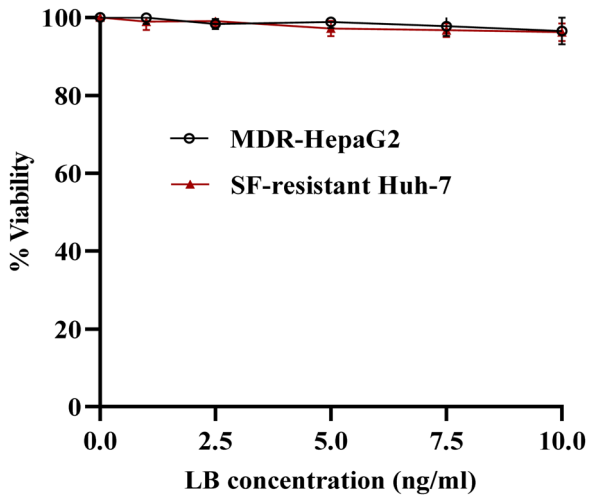

Fig. 6 *In vitro* cytotoxicity of LB against MDR-HepaG2 and SF-resistant Huh-7 cells after 24 h of incubation.

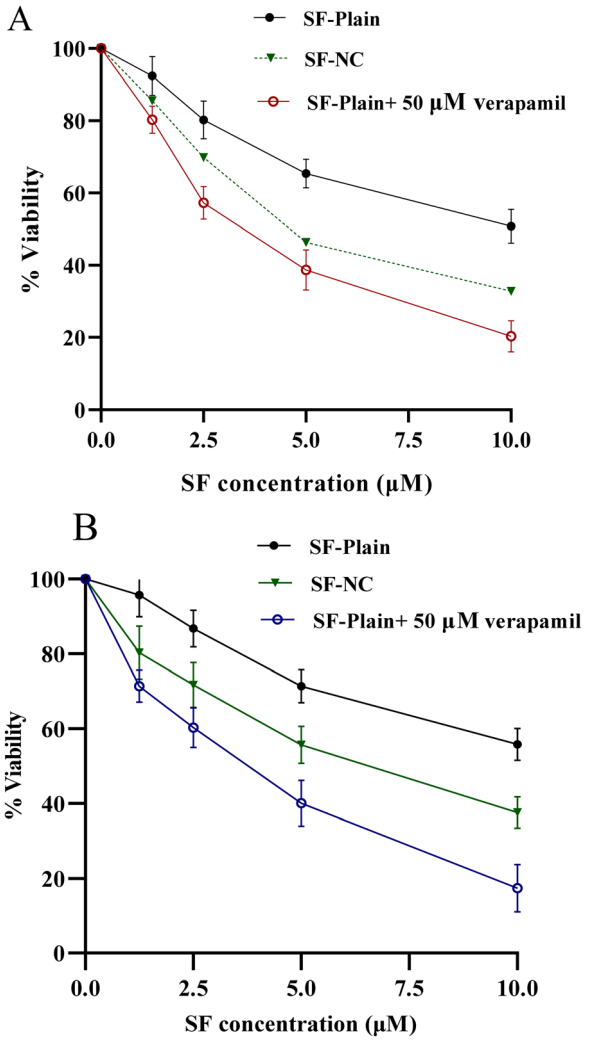

Fig. 7 The cytotoxicity of SF-plain, SF-NC (F2), and SF-plain + 50 μM against MDR-HepG2 (A), and SF-resistant Huh-7 (B) cells after 24 h incubation. The measurements were taken using MTT cell viability assay. The data represent mean ± S.D. of three independent experiments.

Notably, when different concentrations of SF-plain crystals were combined with 50 μM verapamil, a remarkable decrease in IC_{50} values to 4.99 ± 0.53 and 4.81 ± 0.66 μM in the case of MDR HepG2 and SF-resistant Huh7 cells, respectively compared to either SF-plain crystals or SF-NC formulation. This reduction can be attributed to the presence of verapamil, which is known as a *P*-gp inhibitor capable of completely reversing the resistance caused by the *P*-gp efflux pump.[57] Although the SF-NC formulation achieved a relatively higher IC_{50} value than the SF-plain + 50 μM verapamil, it still demonstrated significantly

Table 2 IC_{50} values (μM ± SD) of SF-plain crystals and SF-NC formulation (F2) against MDR-HepG2, and SF-resistant Huh-7, calculated after 24 h exposure

	IC_{50} (Mean ± SD μM)		
Cancer cells	SF-plain crystals	SF-NC (F2)	SF-plain + verapamil
MDR-HepG2	9.60 ± 1.07	6.31 ± 0.71	4.99 ± 0.53
SF-resistant Huh-7	10.67 ± 1.30	7.06 ± 0.84	4.81 ± 0.66

The data represent the mean ± SD of three independent experiments.

lower values than the SF-plain. The findings suggest that SF-NC successfully reduces the viability of MDR-HepG2 and SF-resistant Huh-7 cells, although its potency is much less compared to verapamil. Further investigations are needed to assess LB's potential in reducing MDR.

Bioavailability study. Fig. 8 displays the plasma concentration-time profiles of plain SF and SF-NC after administering a single oral dose of 50 mg suspensions. The mean values of bioavailability parameters, including C_{max}, T_{max}, and AUC_{0-24} are presented in Table 3. The mean C_{max} value of the plain SF was 166.475 ± 6.523 μg mL^{-1}, reached after 6 hours compared to 196.4 ± 19.09 μg mL^{-1}, achieved after 4 hours in the case of SF-NC. The mean value of AUC_{0-24} of SF-NC was 2949.4 ± 268.6 μg h mL^{-1} and showed a significant increase when compared to that of plain SF which was 2320.9 ± 79.32 μg h mL^{-1}. The obtained results indicated that formulation of SF-NC, stabilized by LB as a *P*-gp inhibitor, remarkably increased both the rate and extent of oral bioavailability of SF in terms of C_{max} and AUC_{0-24}, as indicated by a 1.27-fold increase in the relative bioavailability. The notable improvements observed in the measured bioavailability parameters were found to have a positive correlation with the results of both *in vitro* dissolution and *in vitro* cytotoxicity studies. These results are well correlated with previous studies regarding the effect of *P*-gp inhibitors on improving intestinal absorption, tissue distribution, and reducing drug elimination, resulting in enhanced oral bioavailability.[67–73] Previous reports indicated that LB enhances drug absorption not only due to the inhibition of

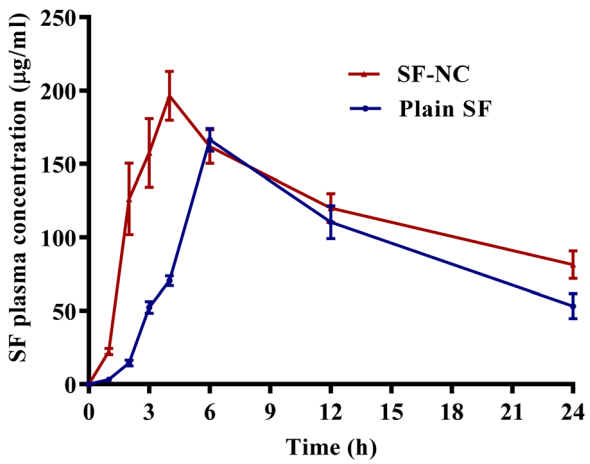

Fig. 8 SF plasma concentration-time profiles (mean ± SD, n = 6) after administration of a single oral dose (50 mg kg^{-1}) of SF-NC and plain SF aqueous suspensions to rats.

Table 3 Bioavailability parameters (mean ± SD, n = 6) after oral administration of 50 mg kg^{-1} as a single dose of ST-NC and plain SF aqueous suspensions

Bioavailability parameters	SF-NC	Plain SF
AUC_{0-24} (μg h mL^{-1})	2949.40 ± 268.60	2320.90 ± 79.32
C_{max} (μg mL^{-1})	196.40 ± 19.09	166.47 ± 6.52
T_{max} (h)	4.00	6.00
Relative bioavailability (%)	127.08%	

P-gp efflux[74] but also increases the cell membrane fluidity,[75] potentiates intestinal absorption of different drugs,[76–78] and alters the permeability in the intestinal "gap junctions".[79]

Conclusion

In conclusion, the results of this study revealed that SF-NC formulation (F2) prepared by 0.02% LB, significantly improved the aqueous saturation solubility and dissolution of SF compared to plain SF. Moreover, *in vitro* cytotoxicity studies showed that LB had no significant effects on the cell viability of MDR-HepaG2 and SF-resistant Huh-7. However, SF-NC significantly reduces IC_{50} values compared to plain SF. *In vivo* absorption studies indicated that formulation of SF-NC, stabilized by LB as a *P*-gp inhibitor, remarkably increased both the rate and extent of oral bioavailability of FS in terms of C_{max} and AUC_{0-24}, as indicated by a 1.27-fold increase in the relative bioavailability. Overall, the developed SF-NC formulation utilizing LB as a stabilizer and *P*-gp inhibitor showed promising improvements in the physicochemical properties and oral bioavailability of SF and could be a reliable strategy for overcoming multidrug resistance in hepatocellular carcinoma cells.

Author contributions

Mohamed Nasr: conceptualization, formal analysis, supervision, writing – reviewing and editing. Sameh Saber: conceptualization, supervision, and visualization. Heba I. Elagamy: methodology, writing – reviewing and editing. Soha M. El-Masry: investigation, methodology, writing and reviewing. Haydy Asad: methodology, writing, and reviewing. Ahmed A. E. M., methodology, Ahmed G. A. G. methodology, Shaimaa K. Mostafa: Methodology, material preparation, data collection, and analysis.

Data availability

Data will be made available on request.

Conflicts of interest

The authors declare that they have no conflicts of interest.

Acknowledgements

This research did not receive any specific grant from funding agencies in the public, commercial, or not-for-profit sectors.

The authors are thankful to Gattefosse (France) for providing the gift samples of Gelucire® 44/14 and Labrasol®.

References

1 F.-H. Kong, Q.-F. Ye, X.-Y. Miao, X. Liu, S.-Q. Huang and L. Xiong, *et al.*, Current status of sorafenib nanoparticle delivery systems in the treatment of hepatocellular carcinoma, *Theranostics*, 2021, **11**(11), 5464.

2 O. Brunetti, A. Gnoni, A. Licchetta, V. Longo, A. Calabrese and A. Argentiero, *et al.*, Predictive and prognostic factors in HCC patients treated with sorafenib, *Medicina*, 2019, **55**(10), 707.

3 M. Monajati, S. Tavakoli, S. S. Abolmaali, G. Yousefi and A. Tamaddon, Effect of PEGylation on assembly morphology and cellular uptake of poly ethyleneimine-cholesterol conjugates for delivery of sorafenib tosylate in hepatocellular carcinoma, *BioImpacts*, 2018, **8**(4), 241.

4 X.-Q. Wang, J.-M. Fan, Y.-O. Liu, B. Zhao, Z.-R. Jia and Q. Zhang, Bioavailability and pharmacokinetics of sorafenib suspension, nanoparticles and nanomatrix for oral administration to rat, *Int. J. Pharm.*, 2011, **419**(1–2), 339–346.

5 S. Jiang, Y. Qin, S. Wu, S. Xu, K. Li and P. Yang, *et al.*, Solubility correlation and thermodynamic analysis of sorafenib free base and sorafenib tosylate in monosolvents and binary solvent mixtures, *J. Chem. Eng. Data*, 2017, **62**(1), 259–267.

6 A. K. Nanayakkara, C. A. Follit, G. Chen, N. S. Williams, P. D. Vogel and J. G. Wise, Targeted inhibitors of *P*-glycoprotein increase chemotherapeutic-induced mortality of multidrug resistant tumor cells, *Sci. Rep.*, 2018, **8**(1), 967.

7 R. N. Montesinos, A. Béduneau, Y. Pellequer and A. Lamprecht, Delivery of *P*-glycoprotein substrates using chemosensitizers and nanotechnology for selective and efficient therapeutic outcomes, *J. Controlled Release*, 2012, **161**(1), 50–61.

8 J. S. Lagas, R. A. van Waterschoot, R. W. Sparidans, E. Wagenaar, J. H. Beijnen and A. H. Schinkel, Breast cancer resistance protein and *P*-glycoprotein limit sorafenib brain accumulation, *Mol. Cancer Ther.*, 2010, **9**(2), 319–326.

9 A. Karbownik, D. Szkutnik-Fiedler, T. Grabowski, A. Wolc, J. Stanisławiak-Rudowicz and R. Jaźwiec, *et al.*, Pharmacokinetic drug interaction study of Sorafenib and morphine in rats, *Pharmaceutics*, 2021, **13**(12), 2172.

10 X. Wang, X. Zhang, X. Huang, Y. Li, M. Wu and J. Liu, The drug–drug interaction of sorafenib mediated by *P*-glycoprotein and CYP3A4, *Xenobiotica*, 2016, **46**(7), 651–658.

11 W. Tang, Z. Chen, W. Zhang, Y. Cheng, B. Zhang and F. Wu, *et al.*, The mechanisms of sorafenib resistance in hepatocellular carcinoma: theoretical basis and therapeutic aspects, *Signal Transduction Targeted Ther.*, 2020, **5**(1), 87.

12 M. Chen, C. Neul, E. Schaeffeler, F. Frisch, S. Winter and M. Schwab, *et al.*, Sorafenib activity and disposition in liver cancer does not depend on organic cation transporter 1, *Clin. Pharm. Ther.*, 2020, **107**(1), 227–237.

13 A. Vasilyeva, S. Durmus, L. Li, E. Wagenaar, S. Hu and A. A. Gibson, *et al.*, Hepatocellular shuttling and recirculation of sorafenib-glucuronide is dependent on Abcc2, Abcc3, and Oatp1a/1b, *Cancer Res.*, 2015, **75**(13), 2729–2736.

14 Y. Shibayama, K. Nakano, H. Maeda, M. Taguchi, R. Ikeda and M. Sugawara, *et al.*, Multidrug resistance protein 2 implicates anticancer drug-resistance to sorafenib, *Biol. Pharm. Bull.*, 2011, **34**(3), 433–435.

15 J. P. Rigalli, N. Ciriaci, A. Arias, M. P. Ceballos, S. S. M. Villanueva and M. G. Luquita, *et al.*, Regulation of multidrug resistance proteins by genistein in a hepatocarcinoma cell line: impact on sorafenib cytotoxicity, *PLoS One*, 2015, **10**(3), e0119502.

16 C. D. Klaassen and L. M. Aleksunes, Xenobiotic, bile acid, and cholesterol transporters: function and regulation, *Pharmacol. Rev.*, 2010, **62**(1), 1–96.

17 S. Ghassabian, T. Rawling, F. Zhou, M. R. Doddareddy, B. N. Tattam and D. E. Hibbs, *et al.*, Role of human CYP3A4 in the biotransformation of sorafenib to its major oxidized metabolites, *Biochem. Pharm.*, 2012, **84**(2), 215–223.

18 P. H. Cui, T. Rawling, T. B. Gillani, K. Bourget, X.-S. Wang and F. Zhou, *et al.*, Anti-proliferative actions of *N*′-desmethylsorafenib in human breast cancer cells, *Biochem. Pharm.*, 2013, **86**(3), 419–427.

19 A. Aman, S. Ali, P. Mahalapbutr, K. Krusong, P. Wolschann and T. Rungrotmongkol, Enhancing solubility and stability of sorafenib through cyclodextrin-based inclusion complexation: in silico and in vitro studies, *RSC Adv.*, 2023, **13**(39), 27244–27254.

20 C. Lim, D. Lee, M. Kim, S. Lee, Y. Shin and J. D. Ramsey, *et al.*, Development of a sorafenib-loaded solid self-nanoemulsifying drug delivery system: Formulation optimization and characterization of enhanced properties, *J. Drug Delivery Sci. Technol.*, 2023, **82**, 104374.

21 N. Diddi, S. Kumar, S. Pavani and P. Neelima, Formulation and Evaluation of Liquid Nanocrystals of Sorafenib Tosylate, *Global J. Pharm. Pharm. Sci.*, 2019, **7**(4), 137–142.

22 D. H. Truong, T. H. Tran, T. Ramasamy, J. Y. Choi, H.-G. Choi and C. S. Yong, *et al.*, Preparation and characterization of solid dispersion using a novel amphiphilic copolymer to enhance dissolution and oral bioavailability of sorafenib, *Powder Technol.*, 2015, **283**, 260–265.

23 S. Xingjie, Y. Zhankuan, Y. Chaofeng and L. Chuanjun, The preparation and characterization of sorafenib solid dispersion, *J. Pharm. Practice Service*, 2016, **34**(4), 320–342.

24 S. Yang, B. Zhang, X. Gong, T. Wang, Y. Liu and N. Zhang, In vivo biodistribution, biocompatibility, and efficacy of sorafenib-loaded lipid-based nanosuspensions evaluated experimentally in cancer, *Int. J. Nanomed.*, 2016, 2329–2343.

25 J. Zhang, T. Wang, S. Mu, L. D. Olerile, X. Yu and N. Zhang, Biomacromolecule/lipid hybrid nanoparticles for controlled delivery of sorafenib in targeting hepatocellular carcinoma therapy, *Nanomedicine*, 2017, **12**(8), 911–925.

26 E. F. Craparo, C. Sardo, R. Serio, M. G. Zizzo, M. L. Bondì and G. Giammona, *et al.*, Galactosylated polymeric carriers for liver targeting of sorafenib, *Int. J. Pharm.*, 2014, **466**(1–2), 172–180.

27 G. Babos, E. Biró, M. Meiczinger and T. Feczkó, Dual drug delivery of sorafenib and doxorubicin from PLGA and PEG-PLGA polymeric nanoparticles, *Polymers*, 2018, **10**(8), 895.
28 J. Varshosaz, F. Raghami, M. Rostami and A. Jahanian, PEGylated trimethylchitosan emulsomes conjugated to octreotide for targeted delivery of sorafenib to hepatocellular carcinoma cells of HepG2, *J. Liposome Res.*, 2019, **29**(4), 383–398.
29 L. Zheng, X. Huang, X. Lin, W. Lin, F. Yang and T. Chen, Thermosensitive hydrogels for sustained-release of sorafenib and selenium nanoparticles for localized synergistic chemoradiotherapy, *Biomaterials*, 2019, **216**, 119220.
30 Y. Wang, H. Yu, D. Zhang, G. Wang, W. Song and Y. Liu, *et al.*, Co-administration of combretastatin A4 nanoparticles and sorafenib for systemic therapy of hepatocellular carcinoma, *Acta Biomater.*, 2019, **92**, 229–240.
31 M. L. Bondì, C. Botto, E. Amore, M. R. Emma, G. Augello and E. F. Craparo, *et al.*, Lipid nanocarriers containing sorafenib inhibit colonies formation in human hepatocarcinoma cells, *Int. J. Pharm.*, 2015, **493**(1–2), 75–85.
32 J.-Y. Wang, Y.-Q. Song, J. Peng and H.-L. Luo, Nanostructured lipid carriers delivering Sorafenib to enhance immunotherapy induced by doxorubicin for effective esophagus cancer therapy, *ACS Omega*, 2020, **5**(36), 22840–22846.
33 H. Tang, D. Chen, C. Li, C. Zheng, X. Wu and Y. Zhang, *et al.*, Dual GSH-exhausting sorafenib loaded manganese-silica nanodrugs for inducing the ferroptosis of hepatocellular carcinoma cells, *Int. J. Pharm.*, 2019, **572**, 118782.
34 J. Ye, R. Zhang, W. Chai and X. Du, Low-density lipoprotein decorated silica nanoparticles co-delivering sorafenib and doxorubicin for effective treatment of hepatocellular carcinoma, *Drug Delivery*, 2018, **25**(1), 2007–2014.
35 A. Grillone, E. R. Riva, A. Mondini, C. Forte, L. Calucci and C. Innocenti, *et al.*, Active targeting of sorafenib: preparation, characterization, and in vitro testing of drug-loaded magnetic solid lipid nanoparticles, *Adv. Healthcare Mater.*, 2015, **4**(11), 1681–1690.
36 S. Benizri, L. Ferey, B. Alies, N. Mebarek, G. Vacher and A. Appavoo, *et al.*, Nucleoside-lipid-based nanocarriers for sorafenib delivery, *Nanoscale Res. Lett.*, 2018, **13**, 1–8.
37 L. Tunki, H. Kulhari, L. N. Vadithe, M. Kuncha, S. Bhargava and D. Pooja, *et al.*, Modulating the site-specific oral delivery of sorafenib using sugar-grafted nanoparticles for hepatocellular carcinoma treatment, *Eur. J. Pharm. Sci.*, 2019, **137**, 104978.
38 Y. Lu, Y. Li and W. Wu, Injected nanocrystals for targeted drug delivery, *Acta Pharm. Sin. B*, 2016, **6**(2), 106–113.
39 A. Tuomela, P. Liu, J. Puranen, S. Rönkkö, T. Laaksonen and G. Kalesnykas, *et al.*, Brinzolamide nanocrystal formulations for ophthalmic delivery: reduction of elevated intraocular pressure in vivo, *Int. J. Pharm.*, 2014, **467**(1–2), 34–41.
40 M. Kurakula, A. El-Helw, T. R. Sobahi and M. Y. Abdelaal, Chitosan based atorvastatin nanocrystals: effect of cationic charge on particle size, formulation stability, and in vivo efficacy, *Int. J. Nanomed.*, 2015, 321–334.
41 P. Liu, X. Rong, J. Laru, B. van Veen, J. Kiesvaara and J. Hirvonen, *et al.*, Nanosuspensions of poorly soluble drugs: preparation and development by wet milling, *Int. J. Pharm.*, 2011, **411**(1–2), 215–222.
42 H. Rahim, A. Sadiq, S. Khan, M. A. Khan, S. M. H. Shah and Z. Hussain, *et al.*, Aceclofenac nanocrystals with enhanced in vitro, in vivo performance: formulation optimization, characterization, analgesic and acute toxicity studies, *Drug Des., Dev. Ther.*, 2017, 2443–2452.
43 M. Nasr, Influence of microcrystal formulation on in vivo absorption of celecoxib in rats, *AAPS PharmSciTech*, 2013, **14**, 719–726.
44 O. Dubray, V. Jannin, F. Demarne, Y. Pellequer, A. Lamprecht and A. Béduneau, In-vitro investigation regarding the effects of Gelucire® 44/14 and Labrasol® ALF on the secretory intestinal transport of *P*-gp substrates, *Int. J. Pharm.*, 2016, **515**(1–2), 293–299.
45 Y. Lin, Q. Shen, H. Katsumi, N. Okada, T. Fujita and X. Jiang, *et al.*, Effects of Labrasol and other pharmaceutical excipients on the intestinal transport and absorption of rhodamine 123, a P-glycoprotein substrate, in rats, *Biol. Pharm. Bull.*, 2007, **30**(7), 1301–1307.
46 K. Sachs-Barrable, A. Thamboo, S. D. Lee and K. M. Wasan, Lipid excipients Peceol and Gelucire 44/14 decrease *P*-glycoprotein mediated efflux of rhodamine 123 partially due to modifying *P*-glycoprotein protein expression within Caco-2 cells, *J. Pharm. Pharm. Sci.*, 2007, **10**(3), 319–331.
47 V. R. Gupta, S. Mutalik, M. M. Patel and G. K. Jani, Spherical crystals of celecoxib to improve solubility, dissolution rate and micromeritic properties, *Acta Pharm.*, 2007, **57**(2), 173–184.
48 A. Tan, S. Simovic, A. K. Davey, T. Rades and C. A. Prestidge, Silica-lipid hybrid (SLH) microcapsules: a novel oral delivery system for poorly soluble drugs, *J. Controlled Release*, 2009, **134**(1), 62–70.
49 Y. Liu, C. Sun, Y. Hao, T. Jiang, L. Zheng and S. Wang, Mechanism of dissolution enhancement and bioavailability of poorly water soluble celecoxib by preparing stable amorphous nanoparticles, *J. Pharm. Pharm. Sci.*, 2010, **13**(4), 589–606.
50 R. Panda and K. Kuotsu, Fabrication, characterization, and in vitro evaluation of pegylated glyceride labrasol® nanostructured lipid carrier composites of methotrexate: the pathway to effective cancer therapy, *Asian J. Pharm. Clin. Res.*, 2019, **12**(6), 229–237.
51 P. M.-K. Tang, D.-M. Zhang, N.-H. B. Xuan, S. K.-W. Tsui, M. M.-Y. Waye and S.-K. Kong, *et al.*, Photodynamic therapy inhibits *P*-glycoprotein mediated multidrug resistance via JNK activation in human hepatocellular carcinoma using the photosensitizer pheophorbide a, *Mol. Cancer*, 2009, **8**, 1–12.
52 J. Y. Chan, A. C. Chu and K. P. Fung, Inhibition of P-glycoprotein expression and reversal of drug resistance of human hepatoma HepG2 cells by multidrug resistance gene (mdr1) antisense RNA, *Life Sci.*, 2000, **67**(17), 2117–2124.
53 J. Zhou, M. Liu, R. Aneja, R. Chandra, H. Lage and H. C. Joshi, Reversal of P-glycoprotein-mediated multidrug resistance in cancer cells by the c-Jun NH_2-terminal kinase, *Cancer Res.*, 2006, **66**(1), 445–452.

54 C. Verslype, H. van Malenstein, J. Dekervel, P. Windmolders, L. Libbrecht and R. van Eijsden, *et al.*, Resistance development after long-term sorafenib exposure in hepatocellular cancer cell lines and risk of rebound growth and epithelial to mesenchymal transition, *J. Clin. Oncol.*, 2012, **30**(4_suppl), 216.

55 J. Li, B. Duan, Y. Guo, R. Zhou, J. Sun and B. Bie, *et al.*, Baicalein sensitizes hepatocellular carcinoma cells to 5-FU and Epirubicin by activating apoptosis and ameliorating P-glycoprotein activity, *Biomed. Pharmacother.*, 2018, **98**, 806–812.

56 J. Dong, B. Zhai, W. Sun, F. Hu, H. Cheng and J. Xu, Activation of phosphatidylinositol 3-kinase/AKT/snail signaling pathway contributes to epithelial-mesenchymal transition-induced multi-drug resistance to sorafenib in hepatocellular carcinoma cells, *PLoS One*, 2017, **12**(9), e0185088.

57 M. Huang and G. Liu, The study of innate drug resistance of human hepatocellular carcinoma Bel7402 cell line, *Cancer Lett.*, 1998, **135**(1), 97–105.

58 P. W. Shueng, H. W. Chan, W. C. Lin, D. Y. Kuo and H. Y. Chuang, Orlistat Resensitizes Sorafenib-Resistance in Hepatocellular Carcinoma Cells through Modulating Metabolism, *Int. J. Mol. Sci.*, 2022, **23**(12), 6501.

59 C.-T. Ting, Y.-Y. Cheng and T.-H. Tsai, Preclinical Pharmacokinetic Interaction and Histopathological Analyses of Hedyotis diffusa on Sorafenib in Rats, *ACS Omega*, 2021, **6**(4), 3060–3067.

60 Guideline IHT, Validation of analytical procedures: text and methodology. Q2 (R1), *ICH Harmonised Tripartite*, 2005, **1**(20), 05.

61 S. Fernandez, V. Jannin, S. Chevrier, Y. Chavant, F. Demarne and F. Carrière, In vitro digestion of the self-emulsifying lipid excipient Labrasol® by gastrointestinal lipases and influence of its colloidal structure on lipolysis rate, *Pharm. Res.*, 2013, **30**, 3077–3087.

62 S. Rani, R. Rana, G. K. Saraogi, V. Kumar and U. Gupta, Self-emulsifying oral lipid drug delivery systems: advances and challenges, *AAPS PharmSciTech*, 2019, **20**, 1–12.

63 V. R. Kallakunta, B. B. Eedara, R. Jukanti, R. K. Ajmeera and S. Bandari, A Gelucire 44/14 and labrasol based solid self emulsifying drug delivery system: formulation and evaluation, *J. Pharm. Invest.*, 2013, **43**, 185–196.

64 A. Karataş, N. Yüksel and T. Baykara, Improved solubility and dissolution rate of piroxicam using gelucire 44/14 and labrasol, *Il Farmaco*, 2005, **60**(9), 777–782.

65 A. A. Noyes and W. R. Whitney, The rate of solution of solid substances in their own solutions, *J. Am. Chem. Soc.*, 1897, **19**(12), 930–934.

66 P. Á. Spósito, A. L. Mazzeti, K. C. M. P. de Castro, P. F. Mendes, J. A. Urbina and M. T. Bahia, *et al.*, Higher oral efficacy of ravuconazole in self-nanoemulsifying systems in shorter treatment in experimental chagas disease, *Exp. Parasitol.*, 2021, **228**, 108142.

67 M. V. Varma, Y. Ashokraj, C. S. Dey and R. Panchagnula, P-glycoprotein inhibitors and their screening: a perspective from bioavailability enhancement, *Pharmacol. Res.*, 2003, **48**(4), 347–359.

68 Y. Kono, I. Kawahara, K. Shinozaki, I. Nomura, H. Marutani and A. Yamamoto, *et al.*, Characterization of P-glycoprotein inhibitors for evaluating the effect of P-glycoprotein on the intestinal absorption of drugs, *Pharmaceutics*, 2021, **13**(3), 388.

69 J. Van Asperen, O. Van Tellingen, A. Sparreboom, A. Schinkel, P. Borst and W. Nooijen, *et al.*, Enhanced oral bioavailability of paclitaxel in mice treated with the P-glycoprotein blocker SDZ PSC 833, *Br. J. Cancer*, 1997, **76**(9), 1181–1183.

70 R. P. Keller, H. J. Altermatt, P. Donatsch, H. Zihlmann, J. A. Laissue and P. C. Hiestand, Pharmacologic interactions between the resistance-modifying cyclosporine sdz psc 833 and etoposide (VP 16–213) enhance In Vivo cytostatic activity and toxicity, *Int. J. Cancer*, 1992, **51**(3), 433–438.

71 J.-O. Kwak, S. H. Lee, G. S. Lee, M. S. Kim, Y.-G. Ahn and J. H. Lee, *et al.*, Selective inhibition of MDR1 (ABCB1) by HM30181 increases oral bioavailability and therapeutic efficacy of paclitaxel, *Eur. J. Pharmacol.*, 2010, **627**(1–3), 92–98.

72 J. Hendrikx, J. Lagas, E. Wagenaar, H. Rosing, J. Schellens and J. Beijnen, *et al.*, Oral co-administration of elacridar and ritonavir enhances plasma levels of oral paclitaxel and docetaxel without affecting relative brain accumulation, *Br. J. Cancer*, 2014, **110**(11), 2669–2676.

73 M. V. Varma and R. Panchagnula, Enhanced oral paclitaxel absorption with vitamin E-TPGS: effect on solubility and permeability in vitro, in situ and in vivo, *Eur. J. Pharm. Sci.*, 2005, **25**(4–5), 445–453.

74 Y. Lin, Q. Shen, H. Katsumi, N. Okada, T. Fujita and X. Jiang, *et al.*, Effects of Labrasol and other pharmaceutical excipients on the intestinal transport and absorption of rhodamine 123, a P-glycoprotein substrate, in rats, *Biol. Pharm. Bull.*, 2007, **30**(7), 1301–1307.

75 K. Koga, S. Kawashima and M. Murakami, In vitro and in situ evidence for the contribution of Labrasol® and Gelucire 44/14 on transport of cephalexin and cefoperazone by rat intestine, *Eur. J. Pharm. Biopharm.*, 2002, **54**(3), 311–318.

76 S. Eaimtrakarn, Y. Rama Prasad, T. Ohno, T. Konishi, Y. Yoshikawa and N. Shibata, *et al.*, Absorption enhancing effect of labrasol on the intestinal absorption of insulin in rats, *J. Drug Targeting*, 2002, **10**(3), 255–260.

77 Z. Hu, R. Tawa, T. Konishi, N. Shibata and K. Takada, A novel emulsifier, Labrasol, enhances gastrointestinal absorption of gentamicin, *Life Sci.*, 2001, **69**(24), 2899–2910.

78 Y. R. Prasad, S. Puthli, S. Eaimtrakarn, M. Ishida, Y. Yoshikawa and N. Shibata, *et al.*, Enhanced intestinal absorption of vancomycin with Labrasol and D-α-tocopheryl PEG 1000 succinate in rats, *Int. J. Pharm.*, 2003, **250**(1), 181–190.

79 X. Sha, G. Yan, Y. Wu, J. Li and X. Fang, Effect of self-microemulsifying drug delivery systems containing Labrasol on tight junctions in Caco-2 cells, *Eur. J. Pharm. Sci.*, 2005, **24**(5), 477–486.